

Research



Cite this article: Gheorghiu A, Coveney PV, Arabi AA. 2020 The influence of base pair tautomerism on single point mutations in aqueous DNA. *Interface Focus* **10**: 20190120. <http://dx.doi.org/10.1098/rsfs.2019.0120>

Accepted: 24 August 2020

One contribution of 9 to a theme issue 'Computational biomedicine. Part I: molecular medicine'.

Subject Areas:

computational biology, biochemistry

Keywords:

high-performance computing, DNA mutation, proton transfer, multiscale modelling

Authors for correspondence:

P. V. Coveney

e-mail: p.v.coveney@ucl.ac.uk

A. A. Arabi

e-mail: alya.arabi@dal.ca

Electronic supplementary material is available online at <https://doi.org/10.6084/m9.figshare.c.5113667>.

The influence of base pair tautomerism on single point mutations in aqueous DNA

A. Gheorghiu¹, P. V. Coveney^{1,2} and A. A. Arabi^{1,3}

¹Centre for Computational Science, University College London, London, UK

²Informatics Institute, University of Amsterdam, Amsterdam, The Netherlands

³College of Medicine and Health Sciences, Biochemistry Department, United Arab Emirates University, PO Box 17666, Al Ain, United Arab Emirates

AG, 0000-0001-6340-3243; PVC, 0000-0002-8787-7256; AAA, 0000-0003-3664-314X

The relationship between base pair hydrogen bond proton transfer and the rate of spontaneous single point mutations at ambient temperatures and pressures in aqueous DNA is investigated. By using an ensemble-based multiscale computational modelling method, statistically robust rates of proton transfer for the A:T and G:C base pairs within a solvated DNA dodecamer are calculated. Several different proton transfer pathways are observed within the same base pair. It is shown that, in G:C, the double proton transfer tautomer is preferred, while the single proton transfer process is favoured in A:T. The reported range of rate coefficients for double proton transfer is consistent with recent experimental data. Notwithstanding the approximately 1000 times more common presence of single proton transfer products from A:T, observationally there is bias towards G:C to A:T mutations in a wide range of living organisms. We infer that the double proton transfer reactions between G:C base pairs have a negligible contribution towards this bias for the following reasons: (i) the maximum half-life of the G*:C* tautomer is in the range of picoseconds, which is significantly smaller than the milliseconds it takes for DNA to unwind during replication, (ii) statistically, the majority of G*:C* tautomers revert back to their canonical forms through a barrierless process, and (iii) the thermodynamic instability of the tautomers with respect to the canonical base pairs. Through similar reasoning, we also deduce that proton transfer in the A:T base pair does not contribute to single point mutations in DNA.

1. Introduction

Mutations within DNA are crucial to both natural evolution and the occurrence of genetic diseases. Despite the protection of a cellular environment, exposure to various external agents such as free radicals, mutagenic compounds, electric fields, metallic centres or sources of radiation are known to cause mutations in DNA [1–3]. As part of their formulation of the DNA replication process, Watson & Crick [4] proposed that spontaneous mutations may arise as a consequence of base pair mismatching. These replication errors, known as *point mutations*, may naturally occur as a result of several types of mismatches such as wobble base pairing, Hoogsteen base pairing, ionization and tautomerism [5–7]. However, the frequency of each type of replication error is uncertain [8]. The purpose of the present paper is to investigate the kinetics and thermodynamics of base pair tautomerism in a realistic DNA model. The origin of these base pair tautomers is an ongoing subject of investigation that has already been studied by idealized gas phase quantum chemical models [9–19]. Despite this research, proton transfer between base pairs is still not completely understood.

In 1963, Löwdin [20] sought out the biological implication of tautomerism as a consequence of proton tunnelling between DNA base pairs. Protons, obeying the laws of quantum theory, behave like wave packets. Therefore, owing to the

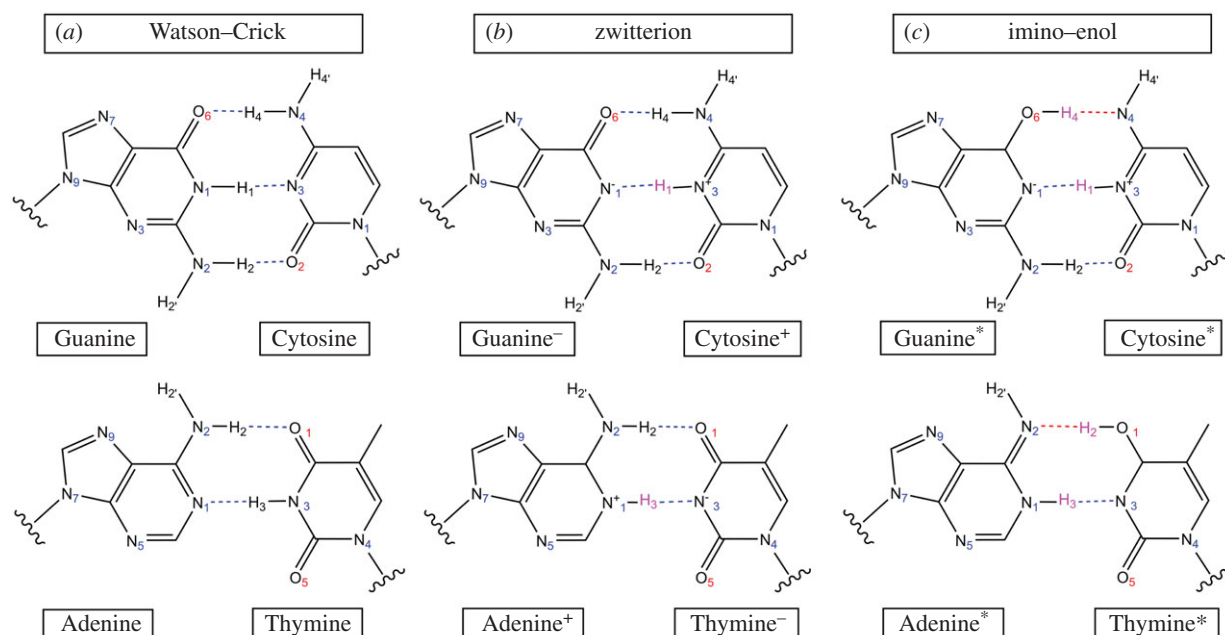


Figure 1. (a) Canonical Watson–Crick base pairs, (b) their single proton transfer zwitterion tautomers and (c) their double proton transfer tautomers (imino–enol). Transferred hydrogen atoms are highlighted in pink.

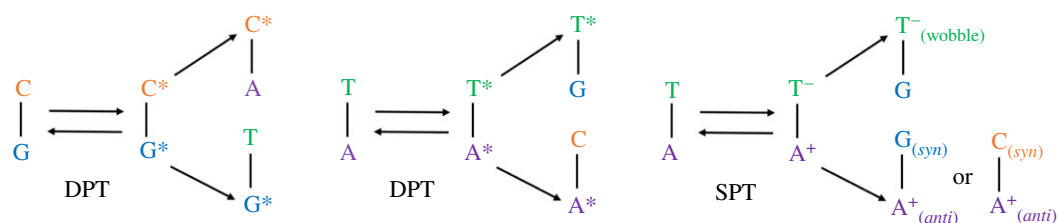


Figure 2. The types of base pair mismatches that may form during the DNA replication process as a consequence of double proton transfer (DPT) and single proton transfer (SPT).

quantum-mechanical (QM) tunnelling effect, there is always a small probability of proton transfer within the hydrogen-bonded network for all base pairs. Some of the products formed of base pair single and double proton transfer are shown in figure 1. Löwdin postulated that this transfer of protons over distances less than 1 Å might be the driving force for genetic mutations in all living organisms.

The proton transfers that occur as a result of hydrogen bonding can also be investigated as an inference of their acid–base chemistry. The pK_a values for the protonation of individual nucleobases in solution have been experimentally determined [21]. However, in the case of base pair hydrogen bonding within aqueous DNA, the ionization state is a function of the surrounding pH gradient [22]. In this study, neutral pH conditions are assumed throughout, which disfavours nucleobase ionization.

In 1976, Topal & Fresco [23] introduced a more comprehensive set of base pairs (other than A:T and G:C) that are consistent with the geometric constraints of the standard double helix. These base pairs included both purine–pyrimidine (e.g. A:C and G:T) and purine–purine (e.g. A:A and G:A) mismatches. An example of how the purine–pyrimidine mismatches may form, as a consequence of base pair proton transfer, is shown in figure 2. A large majority of these base pair mismatches have been experimentally observed within aqueous DNA, in some cases within the active site of the DNA polymerase [6,24–29].

Recent density functional theory (DFT) calculations have shown that, within the approximation of implicit solvent,

single proton transfer is thermodynamically a more favourable process than double proton transfer in the A:T base pair [30]. The single proton transfer A^+T^- zwitterion product facilitates mismatches in the form of wobble base pairing and base flipping (*anti-syn*), all of which do not fit within the restraints of the standard double helix [31–33]. The accurate replication of the Watson–Crick base pairs (G:C and A:T) is partly ensured by their high binding affinity to DNA polymerase [34]. There is a clear distinction in binding affinities to DNA polymerase for T^*G/G^*T and C^*A/A^*C with respect to all other base pair mismatches, which indicates that any other base pair mismatches are more likely to be flagged during the replication process for repair and, thus, not contribute to single point mutation rates [35].

The observed rates of spontaneous mutations must first be measured prior to determining the correlation between base pair tautomerism and spontaneous mutations. The rates of spontaneous mutations for DNA have been experimentally measured in a variety of living organisms, including humans [36,37]. The observed rates of spontaneous mutations in humans are low, estimated to be between 10^{-8} and 10^{-11} base pairs per nucleotide replication or up to 30 base pairs per genome [37–39]. In order to observe the effect of base pair tautomerism on the rate of spontaneous mutations, the equilibrium constant for the process must be greater than or equal to 10^{-8} . This is due to the high-fidelity regulation of DNA repair during replication throughout the cell cycle [40,41].

This paper is divided into five further sections. Section 2 provides an introduction to previous proton transfer models and evaluates their shortcomings. Section 3 outlines the

chemical pathways studied in this work and defines the physico-chemical parameters chosen in this study. Section 4 details the methods used to model DNA on the multiscale, bridging QM and molecular dynamics (MD) methods. The results are displayed in §5, followed by a discussion on the significance of base pair tautomerism for single point mutation rates in DNA. We draw our conclusions in §6.

2. Previous modelling of DNA

A:T and G:C dimers have been modelled with a solvent typically approximated by an implicit polarizable continuum model (PCM) [12,13,42]. One recent DFT study reported that the use of PCM was enough to change the mechanism of double proton transfer in the G:C base pair from concerted to stepwise [16]. Applying the PCM model is a computationally inexpensive way to approximate solvent, but does not capture the detailed local ordering of explicit water molecules around the reaction site of interest. Including realistic aqueous surroundings when modelling DNA is necessary to accurately describe base pair interactions and the proton transfer between them. Indeed, the main contribution to the stabilization of the DNA double helix does not come from inter-base pair hydrogen bonds, but rather from its interaction with surrounding solvent [43]. Within aqueous conditions, the cohesive base pair stacking interactions form a hydrophobic interior which maximizes the hydrogen bonding between base pairs. More recently, some authors have directed their attention towards multiscale modelling approaches to DNA, including in particular the application of QM/molecular mechanics (QM/MM) methods, in some instances further coupled to classical MD [10,44–52]. Several of these studies have investigated the effect of increasing the size of the QM region, including the insertion of explicit water molecules in the inner solvation sphere, the phosphate backbone or the adjacent base pairs [10,50–55]. Through the inclusion of several water molecules in the QM region, a ‘water-assisted’ base pair proton transfer pathway has been observed via Grotthuss-like transition states [50]. However, the activation energy associated with Grotthuss-like transition states is about twice that of direct proton transfer. Such mechanisms contribute to the rate process at higher order and, as we shall show, their effects lie within the errors of the dominant direct mechanism.

3. Description of physico-chemical parameters

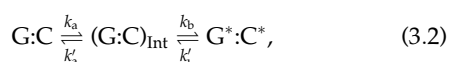
This section displays the five fundamental chemical reactions underpinning base pair tautomerism, including their energetics, rates and equilibrium thermodynamics. These are as follows.

- The tautomerism of the G:C base pair via the concerted double proton transfer mechanism



whereby $\text{G}^*:\text{C}^*$ is the double proton transfer tautomer; the forward and reverse rate coefficients are given by k_r and k'_r , respectively.

- The tautomerism of the G:C base pair via the stepwise double proton transfer mechanism



in which a two-step mechanism involving the formation of a single proton transfer intermediate $(\text{G:C})_{\text{Int}}$ is followed by the production of the $\text{G}^*:\text{C}^*$ tautomer. The rate coefficients pertaining to the first and second steps are embellished by the subscripts ‘a’ and ‘b’, respectively.

- The single proton transfer in the G:C base pair via the concerted mechanism



whereby $\text{G}^-:\text{C}^+$ is the zwitterion product.

- The tautomerism of the A:T base pair via the concerted double proton transfer mechanism



where $\text{A}^*:\text{T}^*$ is the tautomer product.

- The single proton transfer in the A:T base pair via the concerted mechanism



where $\text{A}^+:\text{T}^-$ is the zwitterion product.

The Gibbs free energy of the system is computed starting from the electronic energy, using DFT, with the inclusion of several thermal corrections

$$\Delta G = \Delta E_{\text{corr}} + k_{\text{B}}T - \Delta S_{\text{vib}}T, \quad (3.6)$$

where ΔE_{corr} is the vibrationally corrected electronic energy, k_{B} is the Boltzmann constant, T is the system temperature (300 K) and ΔS_{vib} is the vibrational entropic energy. The electronic energy corrected by quantized vibrations (E_{corr}) is defined as

$$E_{\text{corr}} = \epsilon_0 + E_{\text{vib}} + E_{\text{ZPE}}, \quad (3.7)$$

where ϵ_0 is the electronic energy, E_{vib} is the vibrational energy term and E_{ZPE} is the zero point energy of the system.

According to conventional transition state theory, the rate coefficient of a first-order reaction k will have the following form [56]:

$$k(T) = \kappa(T) \frac{k_{\text{B}}T}{h} \exp\left(-\frac{\Delta G^\ddagger}{RT}\right), \quad (3.8)$$

where T is the temperature (300 K), h is Planck’s constant, ΔG^\ddagger is the Gibbs free energy barrier and R is the universal gas constant. The tunnelling coefficient, $\kappa(T)$, is given by the Wigner correction at second order [57],

$$\kappa(T) = 1 + \frac{1}{24}(\beta\hbar\omega_b)^2; \beta = \frac{1}{k_{\text{B}}T}, \quad (3.9)$$

where ω_b is the imaginary frequency of the transition state.

The equilibrium constant (K) for the reversible first-order reaction $\text{A} \xrightleftharpoons[k'_r]{k_r} \text{B}$ is expressed as

$$K = \frac{k_r}{k'_r}, \quad (3.10)$$

where k_r is the forward rate coefficient and k'_r is the reverse rate coefficient. The half-life ($t_{1/2}$) of the species B is given by

$$t_{1/2} = \frac{\ln 2}{k'_r}. \quad (3.11)$$

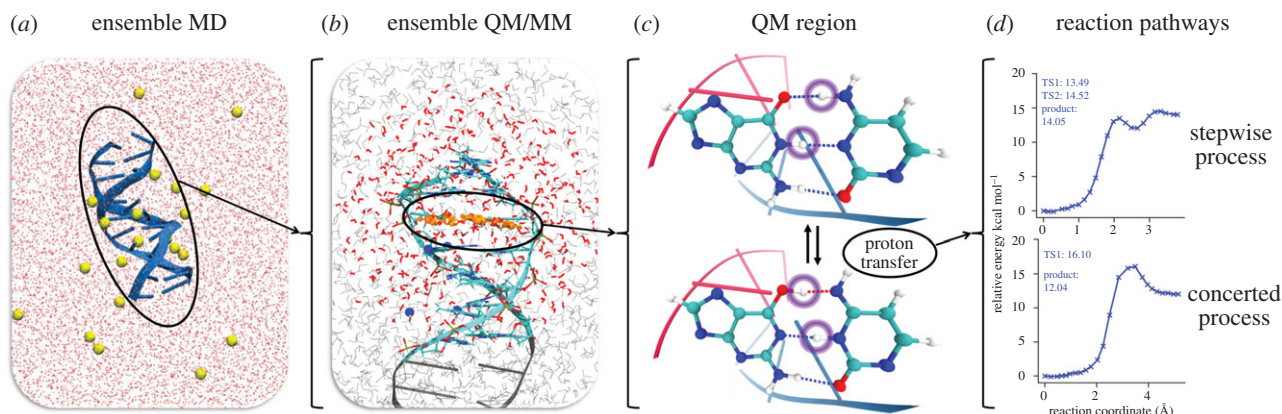


Figure 3. A schematic diagram displaying the multiscale workflow used in this work. (a) Ensemble-based classical molecular dynamics with the AMBER *parmbsc1* force field at 300 K and 1 atm is used to thermalize the DNA dodecamer (NAMMD). (b) Ensemble-based QM/MM starting with initial configurations drawn from prior MD (ChemShell linking NWChem/DL-POLY). (c) The subsequent single base pair QM region (approx. 30 atoms). (d) The proton transfer reaction pathways from which the rate coefficients for the reaction are inferred.

The rate coefficients for a reversible two-step reaction are defined as

$$A \xrightleftharpoons[k'_a]{k_a} I \xrightleftharpoons[k'_b]{k_b} P, \quad (3.12)$$

where A is the reactant, I is an intermediate and P is the product. The equilibrium constant (K) of this two-step reaction can be expressed as

$$K = \frac{k_a}{k'_a} \times \frac{k_b}{k'_b} = K_a \times K_b, \quad (3.13)$$

where K_a and K_b are the respective equilibrium constants for the first and second steps. In the case of $k_a \ll k'_a$, the two-step chemical reaction may be simplified to

$$A \xrightleftharpoons[k'_b]{k'_a} I \xrightleftharpoons[k'_b]{k_b} P. \quad (3.14)$$

Applying a steady-state approximation to the intermediate [I], the rate of the reverse reaction (the consumption of [P]) is expressed as

$$\frac{d[P]}{dt} = -\frac{k'_b k'_a}{k_b + k'_a} [P]. \quad (3.15)$$

Therefore, the overall reverse rate coefficient (k'_r) for the multi-step reaction is approximated to

$$k'_r = \frac{k'_b k'_a}{k_b + k'_a}. \quad (3.16)$$

In equilibrium, the number of tautomeric base pairs per genome, N_{taut} , is given by

$$N_{\text{taut}} = K \times N, \quad (3.17)$$

where N is the size of the genome in base pairs and K is the double proton transfer equilibrium constant. To determine the number of zwitterion base pairs per human genome (N_{zwitter}) at equilibrium, equation (3.17) is applied using the single proton transfer equilibrium constant.

In the case of G:C, the proportion of base pairs converted to tautomers after a certain time is given by the following equation describing the kinetics for a reversible first-order reaction [58]:

$$[G^*C^*]_t = \frac{k_r[GC]_0 - k'_r[G^*C^*]_0}{k_r + k'_r} \{1 - \exp[-(k_r + k'_r)t]\}, \quad (3.18)$$

where $[G^*C^*]_t$ is the concentration of the rare tautomer at time t and k_r and k'_r are the forward and reverse rate coefficients, respectively. The concentrations $\{[GC]_0, [G^*C^*]_0$ and $[G^*C^*]_t\}$ in equation (3.18) are replaced by $\{[AT]_0, [A^+T^-]_0$ and $[A^+T^-]_t\}$ for the case of single proton transfer in the A:T base pair; the subscripts 0 denote the initial time.

4. Multiscale modelling of DNA

Our model begins with the experimentally resolved structure of the B-DNA 'Drew–Dickerson dodecamer' $d(\text{CGCGAATTCGCG})_2$ [59]. Its conformational landscape is explored using ensemble-based classical MD, from which the configurations for the quantum chemical models are drawn. From there, an additional ensemble of quantum mechanics/molecular mechanics is performed to estimate the rates of base-pair proton transfer. A scheme showing the multiscale workflow used in this work is displayed in figure 3.

4.1. Ensemble-based classical molecular dynamics

The reproducibility of MD remains a topic of debate for many theoretical chemists and biologists [60–62]. Because of the extreme sensitivity to the initial conditions in any chaotic MD simulation, one-off simulations are not reliable. Instead, we can obtain statistically robust results by performing ensemble-based simulations, that is, a collection of n replicas each differing from the other solely in terms of the initial velocities assigned to all the atoms, drawn from a Maxwell–Boltzmann distribution at the temperature of interest [62]. Furthermore, ensemble-based simulations provide a reliable means of quantifying uncertainty in general [63].

The *parmbsc1* AMBER force field is used since it performs well for solvated double-helix DNA MD simulations [64,65]. The B-DNA structure of the Drew–Dickerson dodecamer (PDB ID: 1BNA) was neutralized (22 Na^+) and solvated in a water box (dimensions: $71.15 \text{ \AA} \times 73.13 \text{ \AA} \times 85.94 \text{ \AA}$) with the TIP3P water model [59,66]. Ensemble classical MD was then performed under periodic boundary conditions. The cut-off for the interaction distance for both electrostatic and van der Waals calculations was set to 10 \AA . To prevent discontinuities in electrostatic and van der Waals energies, pairs of atoms greater than 11.5 \AA apart were excluded. Periodic boundary electrostatics were calculated using the particle mesh Ewald

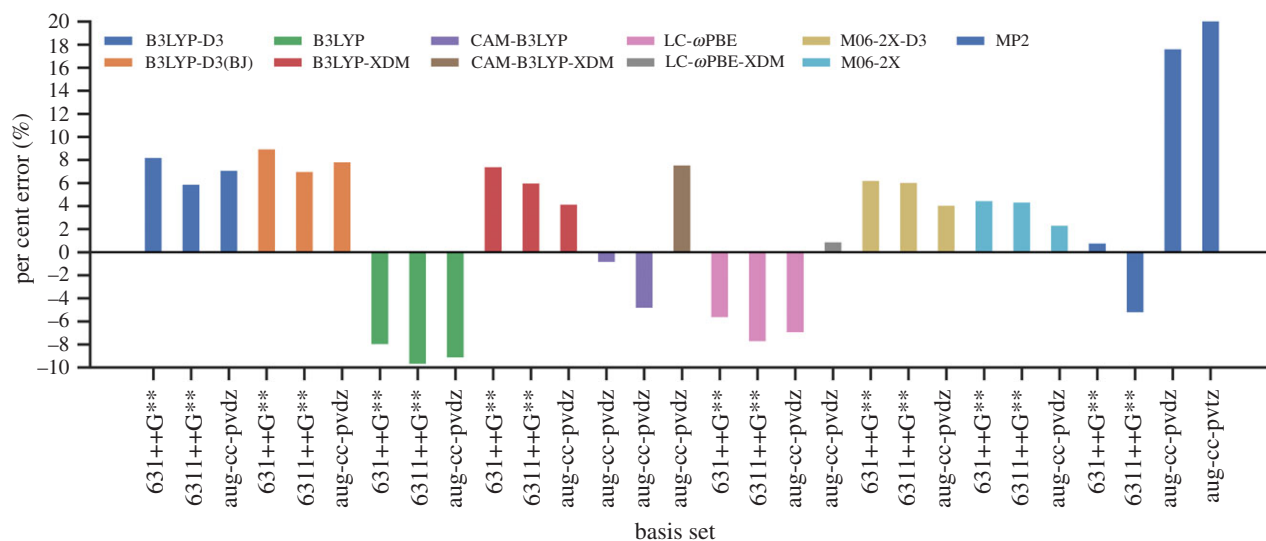


Figure 4. Per cent error in the binding energies of the hydrogen-bonded G:C base pair for a variety of selected QM methods and basis sets compared with the MP2(cc-pvtz)/CCSD(T)[CBS] reference value ($-32.06 \text{ kcal mol}^{-1}$) [71].

method with a grid spacing of 1 \AA . The following equilibration and simulation steps are repeated 10 times using the *parmbsc1* AMBER force field, generating a total of 100 ns simulation for the ensemble.

Equilibration: The coordinates of the entire DNA were restrained as the geometry of the rest of the system was minimized using the conjugate gradient and line search algorithm for 10 000 steps. Next, the temperature of the system was incrementally raised from 50 K to 300 K over a time period of 30 ps with a time step of 1 fs. The temperature of the system was maintained constant using a Berendsen barostat at a pressure of 1 atm. The restraints were then systematically removed over 0.5 ns, followed by an unrestrained 0.5 ns run.

Simulation: The production runs were for 10 ns, simulated at a constant temperature and pressure (300 K, 1 atm). All bonds between heavy atoms and hydrogen were constrained to their nominal length during integration and a time step of 2 fs was employed.

All MD simulations were performed using NAMD 2.12 on the UCL high-performance computing (HPC) facility *Grace*.

4.2. Choosing the quantum-mechanical method

A group of QM methods were compared on their ability to accurately describe base pair geometries and their interaction energies. Various QM methods that are known to accurately describe proton transfer barriers were chosen [67]. The QM methods assessed include B3LYP, CAM-B3LYP, LC- ω PBE, M06-2X and MP2, in conjunction with different basis sets and dispersion corrections. Both double zeta and triple zeta basis sets were assessed in conjunction with a double diffuse function to properly evaluate the energies of hydrogen bonds. To accurately capture weak dispersion interactions between base pairs, the Grimme-D3 correction and the exchange-hole dipole model (XDM) dispersion correction were individually assessed [68–70]. All QM calculations were performed using NWChem 6.6 on the Blue Waters supercomputer at the National Center for Supercomputing Applications, USA.¹

The geometry of a gas phase G:C base pair was optimized using each QM method and the guanine–cytosine interaction energies were calculated. The energies were then compared with highly accurate coupled-cluster values obtained by

Hobza and co-workers [71] (as shown in figure 4). The RMSD of the selected base pair geometries were then compared with an MP2/aug-cc-pvdz optimized G:C base pair (further detailed in electronic supplementary material, S2). Although it is not feasible to use a triple zeta basis set, owing to its computational cost, both the double and triple zeta basis sets were considered in this benchmark for comparison purposes. In general, the triple zeta basis sets are expected to outperform the double zeta basis sets. However, in figure 4, it is shown that this is not the case for the Dunning basis sets in conjunction with the MP2 and CAM-B3LYP method. The same trend can be seen for the Pople basis sets, whereby 6-31++G** outperforms 6-311++G** when used with the B3LYP, LC- ω PBE and MP2 methods. This may be due to the cancellation of errors.

The interaction energies of stacked DNA base pairs were evaluated using B3LYP in combination with different basis sets and dispersion correction schemes. The same protocol as outlined in Šponer and co-workers [72] was followed and the interaction energies for 10 different combinations of stacked base pairs were calculated. A detailed definition of how the interaction energies are defined in addition to the computational methodology applied is offered in electronic supplementary material, S2.2. The results of the benchmark were then compared with the highly accurate DLPNO-CCSD(T)/CBS reference values (table 1). It is demonstrated that the B3LYP+XDM/aug-cc-pvdz binding energies compare well to the reference values for both the two-body and four-body stacking interaction energies. Despite its remarkable accuracy in predicting binding energies of hydrogen-bonded base pairs, CAM-B3LYP fails to accurately predict the binding energies of stacked base pairs.

Therefore, the B3LYP/aug-cc-pvdz with XDM dispersion correction was selected as the QM method in this study, based on its ability to accurately reproduce the binding energies and geometries of both the hydrogen bonded and stacked base pairs (as shown in electronic supplementary material, S2).

4.3. Ensemble quantum mechanics/molecular mechanics

Previous base pair proton transfer studies that use *ab initio* MD are limited by the expense (and therefore the accuracy)

Table 1. The computed average errors for the interaction energies of 10 combinations of stacked base pairs compared with DLPNO-CCSD(T)/CBS reference values [72]. The two-body and four-body stacking energies are given by ΔE_{stack} and $\Delta E_{4\text{stack}}$, respectively.

method	basis sets	average error in	
		ΔE_{stack} (kcal mol ⁻¹)	$\Delta E_{4\text{stack}}$ (kcal mol ⁻¹)
B3LYP+D3	6-31++G**	-1.237	-2.000
	6-311++G**	-1.751	-2.462
	aug-cc-pvdz	-1.459	-2.144
B3LYP+D3(BJ)	6-31++G**	-1.889	-2.651
	6-311++G**	-2.402	-3.113
	aug-cc-pvdz	-2.111	-2.795
B3LYP+XDM	6-31++G**	-1.487	-1.867
	6-311++G**	-2.377	-2.520
	aug-cc-pvdz	0.782	0.345
CAM-B3LYP	6-31++G**	13.785	13.282
	6-311++G**	13.247	12.818
	aug-cc-pvdz	13.658	13.248

of the QM method, by the size of the explicit base pair environment and by the accessible time scale of simulation [44,73,74]. The impracticality and cost of performing multiple *ab initio* MD simulations is obviated by the use of a multiscale ensemble based on the QM/MM method [75]. In this way, the statistical relevance of various proton transfer pathways can be assessed.

Despite numerous studies of DNA using QM/MM methods, there is no single agreed approach to modelling it [10,48–52]. Previous work has shown that the effects of adjacent base pair stacking can modify both the strengths and lengths of base pair hydrogen bonds, which ultimately influence the proton transfer energy profile [30,44,50]. However, a more recent QM/MM study (performed by Das *et al.* [52] in which 10 snapshots from a single MD simulation were studied) showed that adjacent base pair stacking has a relatively small influence on the base pair proton transfer energetic profile of the order of 1 kcal mol⁻¹. The authors investigated the effect of neighbouring base pair polarization by systematically increasing the QM region size from one base pair through to five nucleosides. Of the 10 QM/MM calculations performed, the authors reported the electronic reaction energy for the single proton transfer in the G⁺:C base pair to vary between 7 and 14 kcal mol⁻¹. The relatively large variance they observed (approx. ± 3 kcal mol⁻¹) indicates that the mean reaction energy is largely independent of (i) the QM region size and (ii) the polarization effects of the adjacent base pairs. In other words, the effect of using a larger QM region lies within the uncertainty of the single proton transfer itself.

We also independently considered the benefits that might accrue from increasing the QM region size to include the adjacent nucleotide base pairs. Our findings corroborate those of Das *et al.* In particular, while barrier heights from our one-off QM/MM calculations are lowered slightly, they lie within the errors arising from ensemble averaging of single base pair QM regions.

The initial configurations for the subsequent QM/MM ensemble were selected from the prior classical MD simulations based on the distance between the base pairs (the

distribution of these distances is shown in figure 5). By sampling from the average of this base pair distance distribution, n configurations are selected as starting points for the ensemble QM/MM study. The number of QM/MM replicas (n) is determined in §4.4.

The QM/MM simulations were performed using ChemShell 3.7 to link NWChem 6.6 (QM) with DL-POLY (MM). All of the QM/MM tasks and optimizations were performed using the DL-FIND module as implemented in ChemShell [76]. The periodicity of each initial QM/MM configuration was removed, which resulted in a solvation sphere of 15 Å containing approximately 9000 atoms. The QM region consisted of a single base pair with hydrogen linker atoms placed between the deoxyribose C1' and the corresponding terminal N of the nucleobase. For this work, the electrostatic interactions between the QM and MM regions were modelled using electrostatic embedding. In principle, the use of a polarizable force field might be expected to provide a more realistic charge description at the price of introducing further fitting parameters. The use of such force fields in QM/MM calculations alters energetic calculations by up to *ca* 1 kcal mol⁻¹ [77], while established electrostatic embedding techniques are more robust and computationally efficient than the best currently available counterparts [78]. In accordance with a previous ChemShell QM/MM DNA study [79], our 'active' MM region consists of all residues within 15 Å of the QM base pair; the remaining residues beyond this distance were frozen. This large active MM region was selected to permit structural changes in the phosphate backbone and the inner solvation sphere during geometry optimization. The proton transfer reaction pathways were calculated between the QM/MM optimized base pair and the proton transfer product using the adiabatic climbing image nudged elastic band (CI-NEB) method [80]. Depending on the curvature of the reaction pathway, the replica was then categorized as either a stepwise or concerted process. Transition states on the reaction pathway were further optimized using the dimer method [81] and verified by a single imaginary frequency in the Hessian. When appropriate, the geometry of the reaction pathway intermediate was

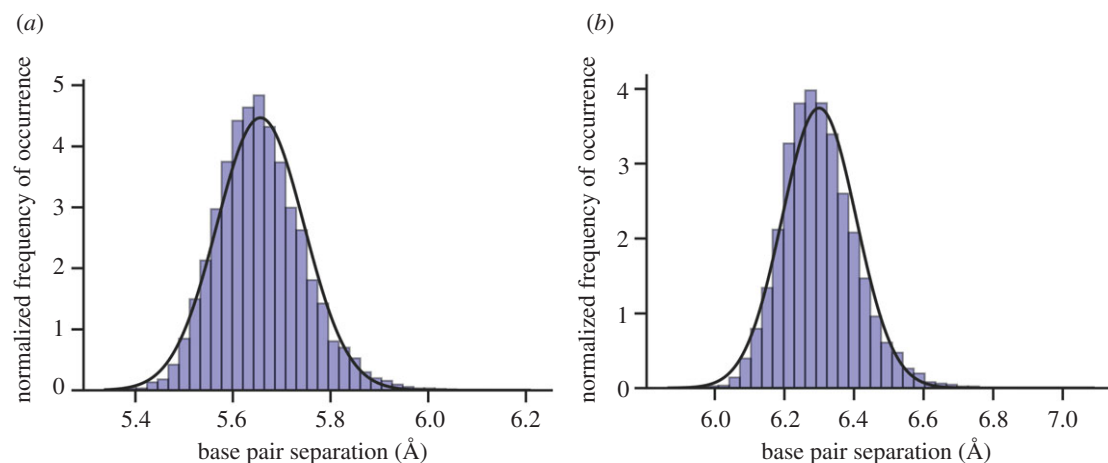


Figure 5. Histogram displaying the normal distribution of mean base pair distances—taken from a total of 100 ns DNA classical molecular dynamics simulation and 10 000 trajectory frames (detailed in §4.1). The continuous lines are the best fit Gaussian representative of the data. (a) G:C base pair (residues 3 and 22), (b) A:T base pair (residues 6 and 19).

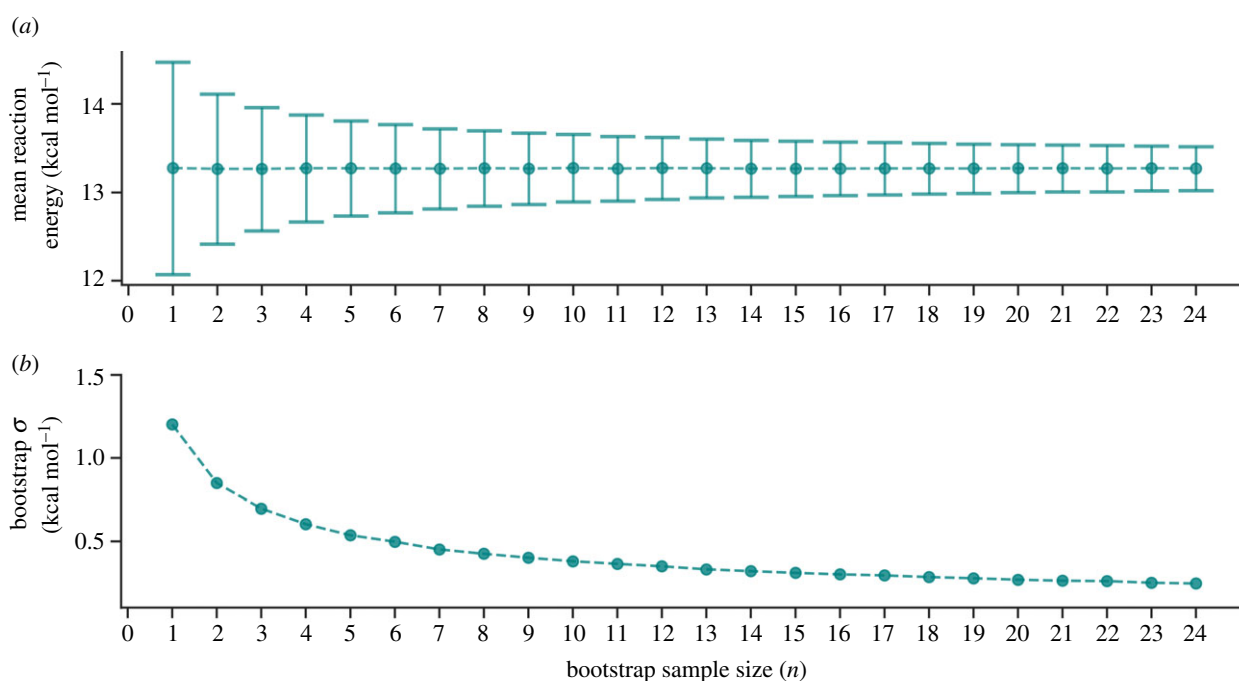


Figure 6. (a) The mean G:C \rightarrow G*:C* tautomerism reaction energy (ΔE_{rxn}) calculated using QM/MM (B3LYP+XDM/aug-cc-pvdz/AMBER). The error bars are the bootstrap standard deviation. (b) The bootstrap standard deviation (σ) of ΔE_{rxn} , plotted against the number of QM/MM replicas n .

optimized to a local minimum. The Hessian for the QM region of each geometry in the optimized proton transfer reaction pathway was then calculated to include thermal corrections of 300 K. Next, the rate coefficients for proton transfer were calculated using conventional transition state theory (equation (3.8)) as implemented in the ChemShell rate module [82]. All ChemShell QM/MM calculations were performed using the UK national supercomputer ARCHER.²

4.4. Uncertainty quantification

To establish an appropriate number of replicas n constituting the QM/MM ensemble, the bootstrap statistical method was employed [63]. By applying the QM/MM methodology as described in §4.3, the reaction energy (ΔE_{rxn}) for the G:C \rightarrow G*:C* tautomerism was calculated per replica. Figure 6 shows that the mean bootstrap standard deviation (σ) for the

reaction energy (ΔE_{rxn}) decreases as the number of replicas (n) increases. After 25 QM/MM replicas are included, the change in σ is negligible and, for this reason, n is set to 25.

5. Results and discussion

Our results show that double proton transfer tautomerism is the most frequent process in the G:C base pair, whereas the A:T base pair favours no reaction, with the subsidiary reaction being single proton transfer. The probability of occurrence for various proton transfer processes is summarized in table 2.

While double proton transfer occurs 96% of the time in the G:C base pair, it was not observed at all in A:T. In fact, no reaction was observed for more than two-thirds (68%) of the A:T replicas. During the geometry optimization of the double proton transfer tautomer product (A*:T*), either one or two

Table 2. The probability of occurrence of the various double proton transfer (DPT) and single proton transfer (SPT) mechanisms observed in the ensemble QM/MM study (sampled from 25 replicas per base pair).

base pair	DPT		SPT		
	concerted	stepwise	concerted	rearrangement	no proton transfer
G:C	0.12	0.84	0.04	0.00	0.00
A:T	0.00	0.00	0.28	0.04	0.68

of the transferred protons were observed to revert back to their original nucleobases, which led to either no overall reaction or single proton transfer. The glaring instability of the A*:T* tautomer is a previously well agreed upon subject, whereby several researchers have instead reported on a metastable A⁺:T⁻ zwitterion intermediate and a highly unstable double proton transfer transition state [10,12,30,74]. In all our cases of single proton transfer in A:T, the same zwitterion product (A⁺:T⁻) was formed.

The double proton transfer process in G:C is split into two different types of pathways: the stepwise mechanism and the concerted mechanism. The probabilities of proton transfer pathways in G:C (as defined in table 2) show that the stepwise process occurs seven times more frequently than the concerted mechanism. Despite the tight restrictions imposed on average base pair distance (obtained from figure 5), the base pair rotation and torsion angles varied significantly between QM/MM replicas. As a consequence of this variation in configurations, many different proton transfer pathways were observed. In particular, one uncommon G:C QM/MM replica displayed the concerted single proton transfer process, while another in A:T (labelled as ‘rearrangement’ in table 2) involved an intra-adenine proton rearrangement. The statistical significance of these pathways is low and can only be thoroughly assessed by a much larger ensemble simulation. Therefore, these rarer cases of proton transfer are excluded from the following analysis, although they do highlight the delicate complexities of the proton transfer reaction pathway overall.

Details of each individual CI-NEB reaction pathway for each replica in the QM/MM ensemble can be found in electronic supplementary material, S3 and S4. The energetics, thermodynamics and kinetics for the three most frequent proton transfer mechanisms in G:C and A:T are shown in table 3.

5.1. G:C tautomerism

The stepwise process is the most probable double proton transfer mechanism in G:C, occurring in 84% of the replicas from the QM/MM ensemble. This process proceeds via two transition states [(G:C)_a[‡], (G:C)_b[‡]] and an intermediate (G:C)_{int}. The less frequent double proton transfer mechanism in G:C is concerted, occurring only 12% of the time. This process proceeds via a single transition state (G:C)[‡] and has a larger electronic energy barrier of approximately 2 kcal mol⁻¹ compared with the stepwise process. The optimized double proton transfer reaction pathways are displayed in figure 7. Tolosa *et al.* [83] were among the rare groups to report more than one possible reaction pathway for the double proton transfer reactions in DNA base pairs. They modelled a microhydrated G:C base pair using M06-2X/6-311++G** and steered MD. They

reported stepwise, concerted and water-assisted mechanisms. The forward barrier height for the first step of the stepwise mechanism is 17.98 kcal mol⁻¹, which is well out of the range we report. In addition, the barrier height they reported for the concerted mechanism was more than twice as high as our reported values.

The energetics, kinetics and thermodynamics for the stepwise double proton transfer mechanism are shown in the left column of table 3. The standard deviation for the mean electronic and Gibbs free energies are consistently approximately 1 kcal mol⁻¹ for each step of the stepwise reaction coordinate. As shown in figure 7 (left), the energy of each part in the reaction coordinate lies within the standard deviation error of all the other points.

On the other hand, only three replicas from the QM/MM ensemble displayed the concerted G:C ⇌ G*:C* tautomerization pathway. The energetics, kinetics and thermodynamics for this pathway are shown in the middle column of table 3. Only three replicas participated in the concerted pathway, indicating the rarity of this phenomenon. As a result, the standard deviation of the energy barrier (ΔE^\ddagger) for the concerted process is twice that of the stepwise.

It is important to note that the overall shape of the double proton transfer reaction profiles, shown in figure 7, changes substantially between electronic and Gibbs free energy. The transition state energies are stabilized by approximately 3.5 kcal mol⁻¹ in terms of the Gibbs free energy. In the case of the stepwise pathway (figure 7, left), this results in the transition states no longer being the maximum relative Gibbs free energies. Consequently, the overall instability of the G*:C* tautomer is reinforced as it occupies the highest Gibbs free energy state on the reaction coordinate. This is due to the zero-point energy contribution stabilizing both stepwise transition states (ΔG_a^\ddagger and ΔG_b^\ddagger) by approximately 2 kcal mol⁻¹ more than the intermediate and products. The computed barrier heights using B3LYP with a dispersion correction are expected to be slightly underestimated (although not to the extent of using B3LYP alone) [84]. The reverse barrier heights for the concerted mechanism in our study are 1.0 ± 1.5 kcal mol⁻¹. These are in good agreement with the values of approximately 1 kcal mol⁻¹ computed using BP86/6-311++G** [42]. Other studies, however, reported reverse free energy barriers less than 0 kcal mol⁻¹ using MP2/aug-cc-pVTZ and B3LYP/6-311++G** [13,15].

The range of the rate coefficients for each step in the G:C base pair stepwise double proton transfer is displayed as a normalized histogram in figure 8. The rate coefficients fit well to the normal distribution of the data, reinforcing the calculated means and standard deviations. The forward rate coefficient for the first step (k_a), shown in orange, is approximately eight orders of magnitude lower than that of the reverse (k'_a), shown in red. The

Table 3. The energies, thermodynamics and rate coefficients for proton transfer reactions in the G:C and A:T base pairs. For the stepwise process, a and b denote the first and second steps, respectively. The electronic energy barriers are denoted by ΔE^\ddagger and reaction energy by ΔE_{rxn} . The Gibbs free energy barriers are denoted by ΔG^\ddagger and the reaction Gibbs energy by ΔG_{rxn} . The forward and reverse rate coefficients of the reaction are given by k_f and k'_f , respectively. The equilibrium constant of the reaction is defined as K. Mean energies are calculated from the QM/MM ensemble using the B3LYP+XDM/aug-cc-pvdz/AMBER method. The standard deviation is denoted by σ . DPT, double proton transfer; SPT, single proton transfer.

	G:C stepwise DPT		G:C concerted DPT		A:T concerted SPT	
	mean	σ	mean	σ	mean	σ
relative electronic energies (kcal mol ⁻¹)						
ΔE^\ddagger	—	—	15.94	2.13	7.13	2.03
ΔE^\ddagger_a	13.98	1.12	—	—	—	—
$\Delta E_{\text{int}}^\ddagger$	13.35	1.18	—	—	—	—
ΔE^\ddagger_b	1.53	0.73	—	—	—	—
ΔE_{rxn}	13.49	1.11	11.72	0.52	6.03	1.92
relative Gibbs free energies (kcal mol ⁻¹)						
ΔG^\ddagger	—	—	12.46	1.86	4.40	2.25
ΔG^\ddagger_a	10.38	1.11	—	—	—	—
$\Delta G_{\text{int}}^\ddagger$	11.41	1.07	—	—	—	—
ΔG^\ddagger_b	0.09	0.64	—	—	—	—
ΔG_{rxn}	12.37	1.31	11.44	0.61	5.49	2.03
rate coefficient (s ⁻¹)						
k_f	—	—	1.19×10^9	1.98×10^9	8.13×10^{10}	9.36×10^{10}
k'_f	7.75×10^{13} , ^a	6.68×10^{13}	7.80×10^{12}	9.14×10^{12}	1.41×10^{14}	5.55×10^{13}
k_a	2.06×10^6	3.38×10^6	—	—	—	—
k'_a	1.17×10^{14}	4.60×10^{13}	—	—	—	—
k_b	1.72×10^{13}	1.27×10^{13}	—	—	—	—
k'_b	8.61×10^{13}	7.51×10^{13}	—	—	—	—
K	5.55×10^{-9}	9.21×10^{-9}	7.99×10^{-9}	8.09×10^{-9}	6.29×10^{-4}	5.55×10^{-4}
K_a	1.55×10^{-8}	2.16×10^{-8}	—	—	—	—
K_b	0.61	0.88	—	—	—	—
half-life, $t_{1/2}$ (s)						
G*:C*	2.37×10^{-14}	2.53×10^{-14}	3.06×10^{-12}	5.12×10^{-12}	—	—
A*:T ⁻	—	—	—	—	6.27×10^{-15}	3.96×10^{-15}

^aCalculated using equation (3.16).

reverse of the first step (G:C)_{int} → G:C is favoured, establishing an equilibrium constant (K_a) of the order of 10^{-8} . The values for the forward (k_b) and reverse (k'_b) rate coefficients, coloured blue and green, respectively (figure 8b), are shown to partially overlap around 10^{13} s⁻¹. The second step of this process (G:C)_{int} ⇌ G*:C* lies close to equilibrium, with a K_b of approximately 0.6. By using equation (3.13), the overall stepwise double proton transfer equilibrium constant (K) is calculated to be of the order of 10^{-9} . Recent computational studies have predicted the G:C double proton transfer equilibrium constant to be between 10^{-6} and 10^{-9} but this is largely dependent on the different QM approximations used [13–16,83,85]. Our results for K (approx. 10^{-9}), are in agreement with Céron-Carrasco & Jacquemin (4.22×10^{-9}) [85], who also used QM/MM methods to simulate proton transfer within a d(GGG)₂ codon. They modelled the central base pair using M06-2X/6-311G**, the stacking base pairs using M06-2X/6-31G* and the sugar-phosphate backbone with the semi-empirical PM6 method. Despite predicting a

similar equilibrium constant, they calculated the respective forward and reverse Gibbs free energy barrier to be 19.54 kcal mol⁻¹ and 8.12 kcal mol⁻¹, which are both approximately 8 kcal mol⁻¹ larger than our results. Céron-Carrasco *et al.* [50] have shown that the inclusion of base pair stacking and explicit solvation causes the double proton transfer equilibrium constant to be smaller than that in the gas phase. In corroboration with their findings, we report equilibrium constants to be one order of magnitude smaller than recent QM-only gas phase studies that have used B3LYP/6-311++G** (1.68×10^{-8}) and MP2/aug-cc-pvTZ (7.5×10^{-8}) methods [13,15].

The rate coefficient of the first forward step (k'_a) is the slowest by several orders of magnitude and, therefore, is the rate-determining step of the stepwise mechanism. For the stepwise process, the half-life of the G*:C* tautomer is calculated to be approximately 20 fs. The equilibrium constant (K) of the concerted mechanism is of the same order of magnitude as the stepwise mechanism (10^{-9}). However, the reverse rate

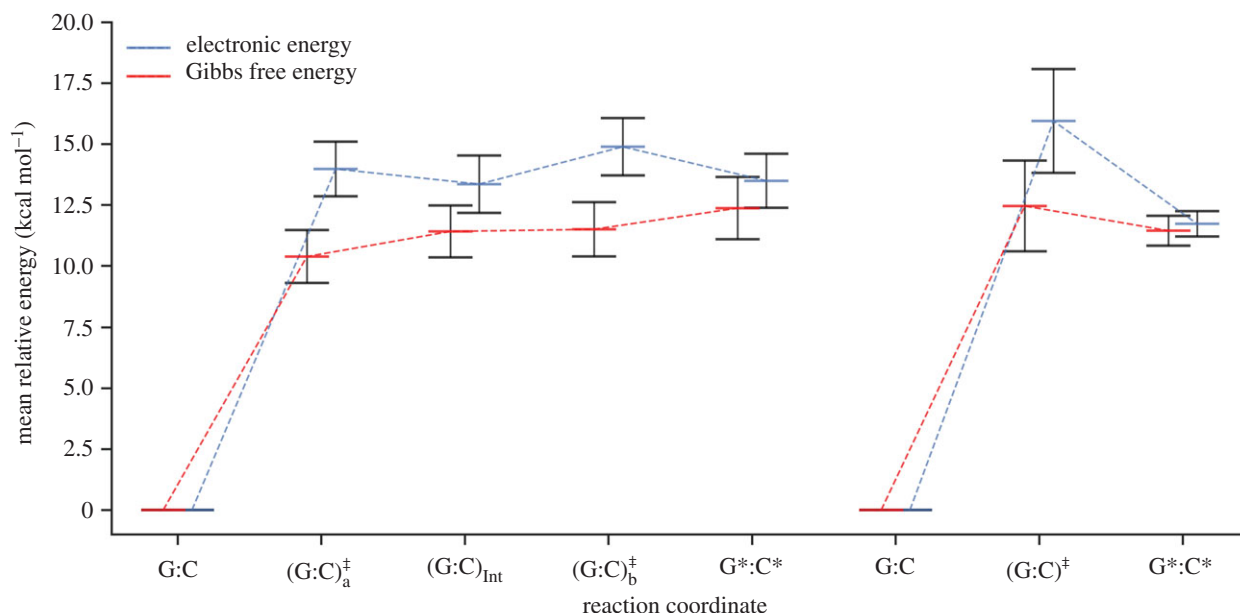


Figure 7. The electronic energy (blue) and the Gibbs free energy (red) as a function of the reaction coordinate for the stepwise (left) and concerted (right) double proton transfer in the G:C base pair. Energies are calculated relative to the energy of the reactant. Error bars are the standard deviations of the mean values.

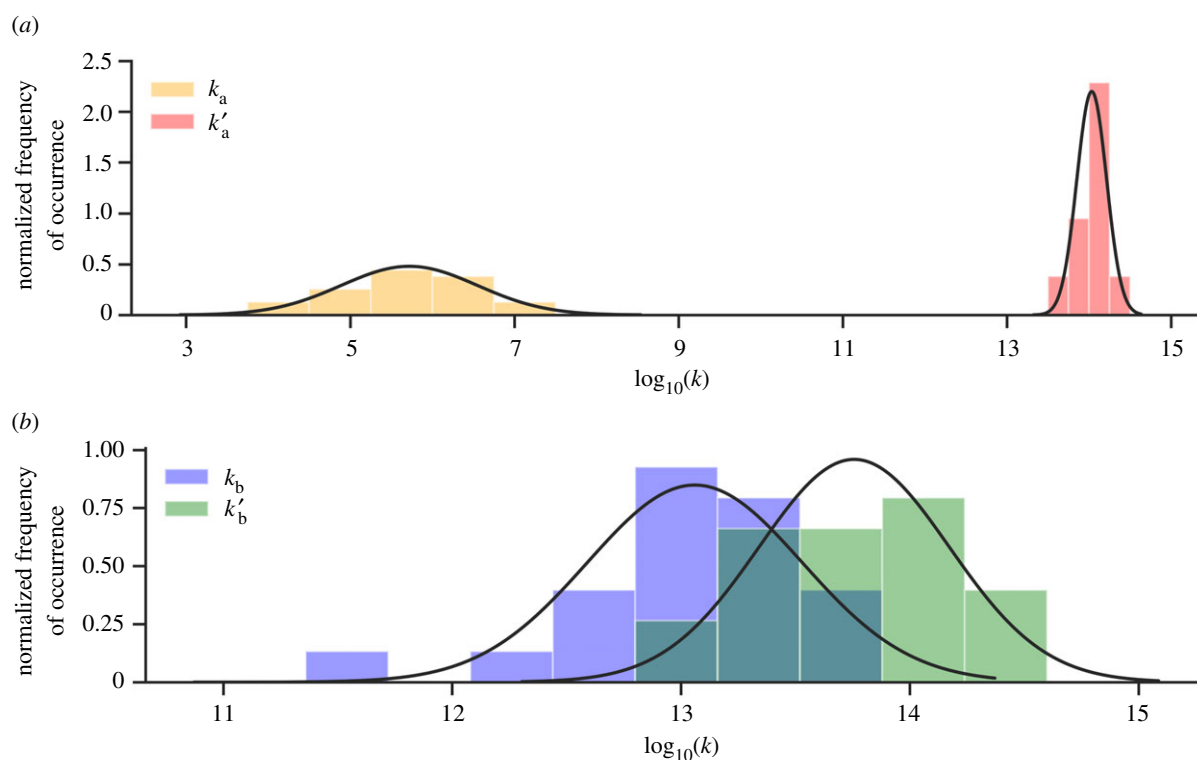


Figure 8. Histogram displaying the normal distribution of the $\log_{10}(k)$ for the stepwise double proton transfer in G:C. (a) The forward k_a (orange) and reverse k'_a (red) rate coefficients of the first step and (b) the forward k_b (blue) and reverse k'_b (green) rate coefficients for the second step. The continuous lines show the best normal distribution fit for each dataset (sampled from 21 QM/MM replicas).

coefficient (k'_a) is roughly two orders of magnitude smaller (approx. 10^{12} s^{-1}) and, consequently, the half-life of the concerted G*:C* tautomer is calculated to be approximately 3 ps.

Previous gas phase base pair double proton transfer studies have typically observed only one of the G:C mechanisms shown in table 2 for a given QM method [10,12,13,17–19,30]. In doing so, the forward rate coefficient for the G:C double proton transfer has been estimated to be between 10^2 and 10^6 s^{-1} , depending on the approximations made and the QM method used [14–16]. Because of the nature of these

QM-only models, the associated errors in measuring the rate coefficient are not reported. A recent nuclear magnetic resonance (NMR) experimental study has estimated the lower bound for the rates of double proton transfer within the (G:T* \rightleftharpoons G*:T) enol tautomerism to be approximately 10^5 s^{-1} or larger [33]. This G:T* base pair mismatch corresponds to guanine connected by three hydrogen bonds to a thymine enol tautomer and is comparatively similar to the G:C base pair. Similarly, the mean forward rate coefficients obtained from our ensemble QM/MM model are 10^6 s^{-1} via the first

step in the stepwise pathway (k_a) and 10^5 s^{-1} via the concerted pathway (k_r). Our results are statistically robust as well as consistent with these experimental data, thus providing substantial improvements on the previous QM calculations.

5.2. A:T tautomerism

For the case of proton transfer occurring in A:T, the greatest percentage of QM/MM replicas (28%) display the concerted single proton transfer reaction. This concerted process involves the transfer of the proton in thymine to adenine to form the $A^+ \cdot T^-$ zwitterion (as shown in figure 1b). The preponderance of single proton transfer over double proton transfer is in agreement with a previous study, which demonstrated that the inclusion of explicit water molecules stabilizes the $A^+ \cdot T^-$ zwitterion over the $A^* \cdot T^*$ tautomer [42].

It should be noted that two of the QM/MM replicas performed have shown that the $A:T \rightarrow A^* \cdot T^*$ double proton transfer reaction pathway can occur, although locating the exact transition states for these replicas was not possible. This is because the electronic energy levels of the approximate transition state and product ($A^* \cdot T^*$) were within close proximity to each other, which resulted in an essentially flat reaction coordinate. Therefore, the transition state geometry optimization was unable to achieve satisfactory gradient convergence for the $A^* \cdot T^*$ tautomerism and the rate coefficients of the reaction were not determined. The $A:T \rightarrow A^* \cdot T^*$ reaction coordinates are displayed in electronic supplementary material, S4. These two replicas were therefore removed from the QM/MM ensemble and replaced by another two, in accordance with the method described in §4.3.

The energetics, kinetics and equilibrium constants for the concerted single proton transfer ($A:T \rightarrow A^+ \cdot T^-$) are presented in the right-hand column of table 3. The mean values and their standard deviations are calculated from a total of seven QM/MM replicas. The reaction coordinate for the concerted single proton transfer in A:T is shown in figure 9. The relative energies of the single proton transfer reaction in A:T (ΔE_{rxn} , ΔG_{rxn}) and the transition state (ΔE^\ddagger , ΔG^\ddagger) are within the standard deviation of one another, similar to that of G:C. The calculated values of the relative transition state energy (ΔE^\ddagger) are unevenly distributed between 5.00 and 11.75 kcal mol⁻¹, resulting in a large standard deviation (approx. 2 kcal mol⁻¹). The Gibbs free energy modifies the single proton transfer reaction coordinate shape (figure 9), by stabilizing the transition state approximately 3 kcal mol⁻¹ more than the $A^+ \cdot T^-$ zwitterion product (ΔG_{rxn}). Several studies have calculated the reverse Gibbs free energy barrier to be 0.5 and 3 kcal mol⁻¹ when using the M05-2X/6-311++G** and the M06-2X/6-311++G** methods, respectively, and in conjunction with the PCM solvent approximation [16,74]. Our work is partially in agreement with an earlier study by Céron-Carrasco *et al.* [30], who used the BP86/6-311++G** method and a micro-hydrated A:T model to predict the reverse free energy barrier to be approximately -1 kcal mol⁻¹. However, the same study predicts the forward Gibbs free energy barrier to be approximately 2 kcal mol⁻¹ smaller than ours (4.4 kcal mol⁻¹). Since there is a distinct lack of QM/MM proton transfer models of A:T in the literature, we expect the difference in our results to be a consequence of the stacking and hydration effects we include. Overall, we find a negative reverse Gibbs free energy barrier for the single proton transfer reaction, which indicates that the $A^+ \cdot T^-$

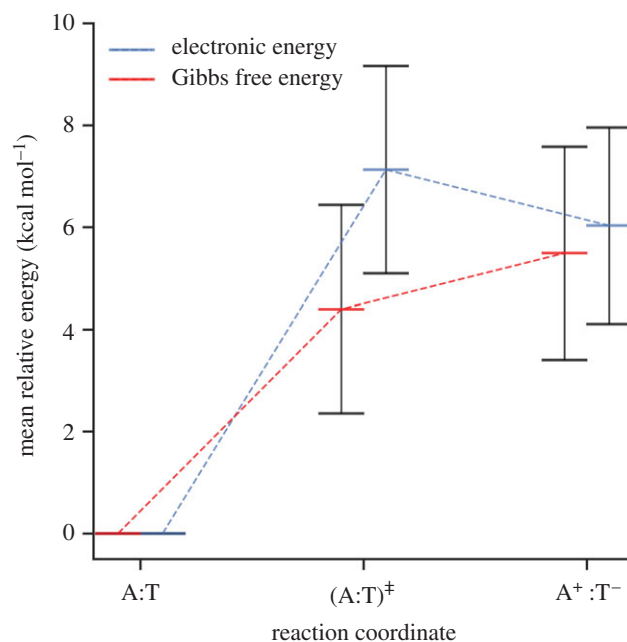


Figure 9. The Gibbs free energy (red) and electronic energy (blue) as a function of the reaction coordinate for the concerted single proton transfer in the A:T base pair. Energies are calculated relative to the energy of the reactant. Error bars are the standard deviations of the mean values.

zwitterion product is energetically unstable relative to the transition state ($A:T$)[‡].

The distribution of the forward (k_r) and reverse (k'_r) rate coefficients for single proton transfer in the A:T base pair is displayed in figure 10. The distribution of k_r (yellow) has a much larger spread than k'_r (red). Because of this, the per cent standard deviation for the forward rate coefficient is much larger than that for the reverse reaction. The mean concerted single proton transfer rate coefficients k_r and k'_r are within the order of 10^{10} and 10^{14} s^{-1} , respectively. The reverse rate coefficient is four orders of magnitude larger than the forward one, resulting in an equilibrium constant (K) for the single proton transfer reaction in A:T of the order of 10^{-4} . From the reverse rate coefficient, the half-life of the $A^+ \cdot T^-$ zwitterion is estimated to be $6.3 \pm 4.0 \text{ fs}$.

5.3. Relation between proton transfer and single point mutation rates

An upper bound on the spontaneous mutation rates in human DNA can be estimated under the following assumptions.

1. The size of the human genome (N) is 3×10^9 bp and comprises purely a 50/50% G:C/A:T content.
2. The spontaneous mutations are exclusively a consequence of the proton transfer mechanisms shown in figure 2 (all other possible mutation pathways were neglected).
3. The single point mutation rates are estimated without consideration of post-replication DNA repair (e.g. proof-reading mechanisms).
4. As a bare minimum, the Gibbs free energy of the tautomer must be lower than the Gibbs free energy of the transition state.
5. For the tautomer to contribute significantly to permanent mutations, the barrier associated with the reverse of proton transfer should be larger than approximately 3 kcal mol⁻¹ [9].

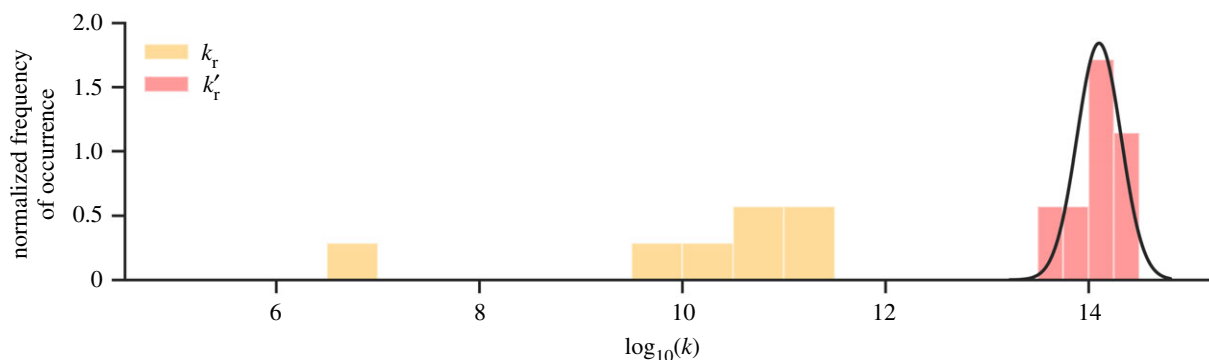


Figure 10. Histogram displaying the normal distribution of the $\log_{10}(k)$ for the concerted single proton transfer in the A:T base pair based on seven replicas. The forward (k_f) and reverse (k_r') rate coefficients are coloured yellow and red respectively. The continuous line shows the best normal distribution fit for the reverse rate coefficient (sampled from seven QM/MM replicas).

Table 4. The equilibrium constant (K), the number of tautomer (N_{taut}) or zwitterion (N_{zwitter}) base pairs per human genome (no. bp) at equilibrium (estimated using equation (3.17)) and the per cent of proton transfer products formed after 1 s (estimated using equation (3.18)). A graphical representation of the tautomer concentrations can be found in electronic supplementary material, S5. DPT, double proton transfer; SPT single proton transfer.

	G:C stepwise DPT		G:C concerted DPT		A:T concerted SPT	
	mean	σ	mean	σ	mean	σ
K	5.55×10^{-9}	9.21×10^{-9}	7.99×10^{-9}	8.09×10^{-9}	6.29×10^{-4}	5.55×10^{-4}
N_{taut} bp	8	14	12	12	—	—
N_{zwitter} bp	—	—	—	—	9.44×10^5	8.32×10^5
% [G* C^*] after 1 s	—	—	7.99×10^{-7}	8.09×10^{-7}	—	—
% [A $^+T^-$] after 1 s	—	—	—	—	6.29×10^{-2}	5.54×10^{-2}
time to reach equilibrium, s	—	—	1.70×10^{-10}	2.30×10^{-10}	3.39×10^{-13}	2.00×10^{-13}

If the above assumptions are satisfied, the proton transfer equilibrium constant (K) is proportional to the number of tautomers at equilibrium and, in turn, the maximum rate of spontaneous mutations per genome. Double proton transfer is assessed independently to single proton transfer, since the two mechanisms and their effect on spontaneous mutation rates *in vivo* are mutually exclusive.

The influence of the G:C double proton transfer reaction on spontaneous mutation rates is detailed in the left and centre columns in table 4. Despite occurring less frequently, the concerted pathway produces 33% more G*:C* tautomers at equilibrium than the stepwise pathway. It is estimated that there are a total of 20 G*:C* tautomers (N_{taut}) within the human genome at equilibrium. It should be noted that the stepwise G*:C* tautomer product has a very short associated half-life (approx. 20 fs; table 3), as well as, on average, a barrierless reverse reaction (-1.0 ± 0.3 kcal mol $^{-1}$ and -0.8 ± 0.6 kcal mol $^{-1}$ for the respective first and second steps). Therefore, in accordance with assumption (4), the stepwise double proton transfer process in G:C is excluded from our single point mutation rate estimate. Given that the concerted tautomerism of G:C has a mean reverse Gibbs energy barrier of 1.0 ± 1.5 kcal mol $^{-1}$, we are not able to say with certainty whether or not the reverse pathway is actually larger than 0 kcal mol $^{-1}$, and thus there is no guarantee that the criterion of assumption (4) is met. Also, keeping in mind that the barrier heights in our study are slightly underestimated, as discussed above, and given that the

3 kcal mol $^{-1}$ threshold in assumption (5) is only an approximation, we are not able to say with certainty whether or not assumption (5) is met. Therefore, we can neither assert that the probabilities of the mutations are null nor affirm that the concerted pathway leads to permanent mutations, especially since the time scale of DNA opening during replication is around one billion times larger [86] than the half-life of the G*:C* tautomer (approx. 3 ps). Therefore, it is reasonable to conclude that only a small fraction of the already small number of G*:C* tautomers (as a consequence of the concerted double proton transfer reaction) may lead to a permanent G:C \rightarrow A:T mutation during DNA replication; in practical terms, it is truly negligible at less than one base pair per human genome replication.

By contrast, the formation of the double proton transfer A*:T* tautomer is rare and was not observed once within the entire QM/MM ensemble. On the other hand, the A:T \rightarrow A $^+T^-$ process was found to be significantly more thermodynamically and kinetically favourable than that of G:C \rightarrow G*:C*. Specifically, there are on average five orders of magnitude more A $^+T^-$ zwitterions than G*:C* tautomers at equilibrium, which contributes towards approximately 0.06% of the A:T content in the human genome. Despite this abundance of A $^+T^-$ content, the zwitterions have a very short half-life (approx. 6 fs), as well as an average barrierless reverse reaction. Therefore, according to assumption (4), the zwitterion is not considered to influence mutation rates during DNA replication.

That G:C base pairs are more likely to spontaneously mutate is consistent with the universal G:C → A:T transition mutation bias observed *in vivo* during the replication process [39,87]. Despite the debate concerning the influence of external agents on this mutation bias, recent studies have reported that spontaneous mutations could be the driving force [88–90]. This bias is also observed in humans, whereby the mutation rate per genome replication for G:C sites is two orders of magnitude faster than for non-G:C sites [38,39]. Similar to recent studies by Brovarets & Hovorun [12,13], our work suggests that the double proton transfer tautomerism reactions in DNA are extremely unlikely to contribute towards the overall rates of transition mutations during the DNA replication process.

6. Conclusion

Through the use of ensemble QM/MM, multiple proton transfer pathways have been observed to occur within the canonical base pairs. We are the first to report a distribution of statistically robust rate coefficients for the most frequently occurring proton transfer mechanisms. The G:C proton transfer rate constants predicted in this paper are in better agreement with recent NMR experimental data than previous simulations [33]. The application of multiscale MD in conjunction with QM/MM enables us to sample realistic configurations for both the A:T and G:C base pairs within DNA under ambient conditions. Our results indicate that previous QM-only models may have oversimplified the processes that are involved in base pair proton transfer.

Both the stepwise and concerted double proton transfer pathways occur within the same G:C base pair. Despite the larger rate constants of the stepwise pathway, the calculated equilibrium constant (*K*) is similar to that of the concerted mechanism (approx. 10^{-9}). As a consequence of both of the pathways, it is estimated that at equilibrium a total of 20 G*:C* tautomers are present in the human genome. However, the fast kinetics of the reverse reaction (G*:C* → G:C) promote the swift reverting of the rare tautomers to canonical G:C. Thus, there is only a negligible chance that the double proton transfer reaction can form G*:C* tautomers that last long enough to have any significant

impact on the rates of point mutations in DNA, especially in the context of human genome replication.

On the other hand, A*:T* tautomerism is not observed in any QM/MM replicas within the ensemble. Indeed, the number of A*:T* tautomers in the human genome at equilibrium is then estimated to be negligible, compared with G*:C*. By contrast, we find that the A⁺:T⁻ zwitterion is 1000 times more likely to occur than the G*:C* tautomer in equilibrium. Despite its relative abundance, the A⁺:T⁻ zwitterion is not expected to cause base pair mismatches owing to its very short half-life (approx. 6 fs) and kinetic/thermodynamic instability.

Data accessibility. The description of input data, structure and trajectory files can be found at <https://github.com/gb3orghiu/>.

Authors' contributions. A.A.A. and P.V.C. provided the overall direction for the project and management in coordination with A.G. The acquisition and management of computational data was undertaken by A.G. All authors contributed to the writing of this article. All authors have approved for this work to be submitted for publication.

Competing interests. We declare we have no competing interest.

Funding. We are grateful to the Engineering and Physical Sciences Research Council (EPSRC), University College London, for funding A.G.'s PhD studentship UK. This project has also received partial funding from Zayed University, United Arab Emirates, the European Union's Horizon 2020 Research and Innovation Programme under grant agreement no. 675451 (CompBioMed) and no. 823712 (CompBioMed2), under grant agreement no. 800925 (VECMA project, <http://www.vecma.eu>), EPSRC under the project 'UK Consortium on Mesoscale Engineering Sciences (UKCOMES)' (grant no. EP/R029598/1), MRC via a Medical Bioinformatics grant (MR/L016311/1) and special funding to P.V.C. from the UCL Provost.

Acknowledgements. We thank You Lu and Thomas Keal at the Science and Technology Facilities Council (STFC), Daresbury, UK, for their support in the use of ChemShell on the ARCHER UK National Supercomputing Service (<http://www.archer.ac.uk>).

Endnotes

¹University of Illinois at Urbana-Champaign, URL: <http://www.ncsa.illinois.edu/>

²EPCC at the University of Edinburgh, URL: <https://www.epcc.ed.ac.uk/facilities/archer>

References

- Li X, Cai Z, Sevilla MD. 2001 Investigation of proton transfer within DNA base pair anion and cation radicals by density functional theory (DFT). *J. Phys. Chem. B* **105**, 10115–10123. (doi:10.1021/jp012364z)
- Walsh JM, Beuning PJ. 2012 Synthetic nucleotides as probes of DNA polymerase specificity. *J. Nucleic Acids* **2012**, 1–17. (doi:10.1155/2012/530963)
- Randall GC, Doyle PS. 2005 DNA deformation in electric fields: DNA driven past a cylindrical obstruction. *Macromolecules* **38**, 2410–2418. (doi:10.1021/ma048073g)
- Watson JD, Crick FHC. 1953 The structure of DNA. *Cold Spring Harb. Symp. Quant. Biol.* **18**, 123–131. (doi:10.1101/SQB.1953.018.01.020)
- Crick FHC. 1966 Codon-anticodon pairing: the wobble hypothesis. *J. Mol. Biol.* **19**, 548–555. (doi:10.1016/S0022-2836(66)80022-0)
- Johnson SJ, Beese LS. 2004 Structures of mismatch replication errors observed in a DNA polymerase. *Cell* **116**, 803–816. (doi:10.1016/S0092-8674(04)00252-1)
- Kimsey IJ. 2016 Visualizing rare Watson-Crick-like tautomeric and anionic mismatches in DNA and RNA. PhD thesis, Duke University, Durham, NC, USA.
- Morgan AR. 1993 Base mismatches and mutagenesis: how important is tautomerism?. *Trends Biochem. Sci.* **18**, 160–163. (doi:10.1016/0968-0004(93)90104-U)
- Florian J, Leszczynski J. 1996 Spontaneous DNA mutations induced by proton transfer in the guanine-cytosine base pairs: an energetic perspective. *J. Am. Chem. Soc.* **118**, 3010–3017. (doi:10.1021/ja951983g)
- Jacquemin D, Zúñiga J, Requena A, Céron-Carrasco JP. 2014 Assessing the importance of proton transfer reactions in DNA. *Acc. Chem. Res.* **47**, 2467–2474. (doi:10.1021/ar500148c)
- Villani G. 2010 Theoretical investigation of hydrogen atom transfer in the cytosine-guanine base pair and its coupling with electronic rearrangement. Concerted vs stepwise mechanism. *J. Phys. Chem. B* **114**, 9653–9662. (doi:10.1021/jp102457s)
- Brovarets OO, Hovorun DM. 2014 Can tautomerization of the A-T Watson-Crick base pair via double proton transfer provoke point mutations during DNA replication? A comprehensive QM and QTAIM analysis. *J. Biomol. Struct. Dyn.* **32**, 127–154. (doi:10.1080/07391102.2012.755795)
- Brovarets OO, Hovorun DM. 2014 Why the tautomerization of the G-C Watson-Crick base pair via the DPT does not cause point mutations during DNA replication? QM and QTAIM comprehensive

- analysis. *J. Biomol. Struct. Dyn.* **32**, 1474–1499. (doi:10.1080/07391102.2013.822829)
14. Cerón-Carrasco JP, Jacquemin D. 2013 Electric-field induced mutation of DNA: a theoretical investigation of the GC base pair. *Phys. Chem. Chem. Phys.* **15**, 4548. (doi:10.1039/c2cp44066k)
 15. Arabi AA, Matta CF. 2018 Effects of intense electric fields on the double proton transfer in the Watson-Crick guanine-cytosine base pair. *J. Phys. Chem. B* **122**, 8631–8641. (doi:10.1021/acs.jpcc.8b05053)
 16. Romero EE, Hernandez FE. 2018 Solvent effect on the intermolecular proton transfer of the Watson and Crick guanine-cytosine and adenine-thymine base pairs: a polarizable continuum model study. *Phys. Chem. Chem. Phys.* **20**, 1198–1209. (doi:10.1039/C7CP05356H)
 17. Villani G. 2006 Theoretical investigation of hydrogen transfer mechanism in the guanine-cytosine base pair. *Chem. Phys.* **324**, 438–446. (doi:10.1016/j.chemphys.2005.11.006)
 18. Godbeer AD, Al-Khalili JS, Stevenson PD. 2015 Modelling proton tunnelling in the adenine-thymine base pair. *Phys. Chem. Chem. Phys.* **17**, 13034–13044. (doi:10.1039/C5CP00472A)
 19. Hayashi T, Mukamel S. 2004 Infrared signatures of proton transfer in guanine-cytosine and adenine-thymine base pairs: Dft study. *Isr. J. Chem.* **44**, 185–191. (doi:10.1560/M6NA-F16J-NVKN-LLM9)
 20. Löwdin PO. 1963 Proton tunneling in DNA and its biological implications. *Rev. Mod. Phys.* **35**, 724–732. (doi:10.1103/RevModPhys.35.724)
 21. Haunschmidt M, Buchberger W, Klampfl CW. 2008 Investigations on the migration behaviour of purines and pyrimidines in capillary electromigration techniques with UV detection and mass spectrometric detection. *J. Chromatogr. A* **1213**, 88–92. (doi:10.1016/j.chroma.2008.09.063)
 22. Thaplyal P, Bevilacqua PC. 2014 Experimental approaches for measuring pKa's in RNA and DNA. In *Riboswitch discovery, structure and function* (ed. DH Burke-Aguero), pp. 189–219. Methods in Enzymology, vol. 549. New York, NY: Academic Press.
 23. Topal MD, Fresco JR. 1976 Complementary base pairing and the origin of substitution mutations. *Nature* **263**, 285–289. (doi:10.1038/263285a0)
 24. Barrett TE, Savva R, Panayotou G, Barlow T, Brown T, Jiricny J, Pearl LH. 1998 Crystal structure of a G:T/U mismatch-specific DNA glycosylase: mismatch recognition by complementary-strand interactions. *Cell* **92**, 117–129. (doi:10.1016/S0092-8674(00)80904-6)
 25. Leonard GA, Booth ED, Brown T. 1990 Structural and thermodynamic studies on the adenine-guanine mismatch in B-DNA. *Nucleic Acids Res.* **18**, 5617–5623. (doi:10.1093/nar/18.19.5617)
 26. Wang W, Hellinga HW, Beese LS. 2011 Structural evidence for the rare tautomer hypothesis of spontaneous mutagenesis. *Proc. Natl Acad. Sci. USA* **108**, 17 644–17 648. (doi:10.1073/pnas.1114496108)
 27. Pan B, Mitra SN, Sundaralingam M. 1998 Structure of a 16-mer RNA duplex r(GCAGACUAAAUCUGC)2 with wobble C-A+ mismatches. *J. Mol. Biol.* **283**, 977–984. (doi:10.1006/jmbi.1998.2140)
 28. Sau AK, Chary KVR, Govil G, Chen Cq, Howard FB, Miles HT. 1995 Evidence for A+(anti)-G(syn) mismatched base-pairing in d-GGTAAGCGTACC. *FEBS Lett.* **377**, 301–305. (doi:10.1016/0014-5793(95)01362-8)
 29. Kimsey IJ, Petzold K, Sathyamoorthy B, Stein ZW, Al-Hashimi HM. 2015 Visualizing transient Watson-Crick-like mispairs in DNA and RNA duplexes. *Nature* **519**, 315–320. (doi:10.1038/nature14227)
 30. Cerón-Carrasco JP, Requena A, Michaux C, Perpète EA, Jacquemin D. 2009 Effects of hydration on the proton transfer mechanism in the adenine-thymine base pair. *J. Phys. Chem. A* **113**, 7892–7898. (doi:10.1021/jp900782h)
 31. Kryachko ES, Sabin JR. 2003 Quantum chemical study of the hydrogen-bonded patterns in A-T base pair of DNA: origins of tautomeric mispairs, base flipping, and Watson-Crick to Hoogsteen conversion. *Int. J. Quantum Chem.* **91**, 695–710. (doi:10.1002/qua.10462)
 32. Brown T, Brown (Jnr) T. 2019 atdbio - Nucleic Acids Book. Available from: <http://www.atdbio.com/nucleic-acids-book>.
 33. Kimsey IJ, Szymanski ES, Zahurancik WJ, Shakya A, Xue Y, Chu CC, Sathyamoorthy B, Suo Z, Al-Hashimi HM. 2018 Dynamic basis for dG:dT misincorporation via tautomerization and ionization. *Nature* **554**, 195–201. (doi:10.1038/nature25487)
 34. Bebenek K, Matsuda T, Masutani C, Hanaoka F, Kunkel TA. 2001 Proofreading of DNA polymerase η -dependent replication errors. *J. Biol. Chem.* **276**, 2317–2320. (doi:10.1074/jbc.C000690200)
 35. Washington MT, Johnson RE, Prakash S, Prakash L. 2001 Mismatch extension ability of yeast and human DNA polymerase η . *J. Biol. Chem.* **276**, 2263–2266. (doi:10.1074/jbc.M009049200)
 36. Drake JW. 1969 Spontaneous mutation: comparative rates of spontaneous mutation. *Nature* **221**, 1132–1132. (doi:10.1038/2211132a0)
 37. Drake JW, Charlesworth B, Charlesworth D, Crow JF. 1998 Rates of spontaneous mutation. *Genet. Soc. Am.* **148**, 1667–1686.
 38. Nachman MW, Crowell SL. 2000 Estimate of the mutation rate per nucleotide in humans. *Genetics* **156**, 297–304.
 39. Kong A *et al.* 2012 Rate of de novo mutations and the importance of father's age to disease risk. *Nature* **488**, 471–475. (doi:10.1038/nature11396)
 40. Showalter AK, Tsai MD. 2002 A reexamination of the nucleotide incorporation fidelity of DNA polymerases. *Biochemistry* **41**, 10 571–10 576. (doi:10.1021/bi026021i)
 41. Branzei D, Foiani M. 2008 Regulation of DNA repair throughout the cell cycle. *Nat. Rev. Mol. Cell Biol.* **9**, 297–308. (doi:10.1038/nrm2351)
 42. Cerón-Carrasco JP, Requena A, Zuñiga J, Michaux C, Perpète EA, Jacquemin D. 2009 Intermolecular proton transfer in microhydrated guanine-cytosine base pairs: a new mechanism for spontaneous mutation in DNA. *J. Phys. Chem. A* **113**, 10 549–10 556. (doi:10.1021/jp906551f)
 43. Feng B *et al.* 2019 Hydrophobic catalysis and a potential biological role of DNA unstacking induced by environment effects. *Proc. Natl Acad. Sci. USA* **116**, 17 169–17 174. (doi:10.1073/pnas.1909122116)
 44. Zoete V, Meuwly M. 2004 Double proton transfer in the isolated and DNA-embedded guanine-cytosine base pair. *J. Chem. Phys.* **121**, 4377–4388. (doi:10.1063/1.1774152)
 45. Gervasio FL, Boero M, Parrinello M. 2006 Double proton coupled charge transfer in DNA. *Angewandte Chemie - Int. Ed.* **45**, 5606–5609. (doi:10.1002/anie.200602106)
 46. Sumowski CV, Ochsenfeld C. 2009 A convergence study of QM/MM isomerization energies with the selected size of the QM Region for peptidic systems. *J. Phys. Chem. A* **113**, 11 734–11 741. (doi:10.1021/jp902876n)
 47. Hitzberger M, Ratanasak M, Parasuk V, Hofer TS. 2016 Optimizing link atom parameters for DNA QM/MM simulations. *Theor. Chem. Acc.* **135**, 1–7. (doi:10.1007/s00214-016-1819-7)
 48. Cerón-Carrasco JP, Cerezo J, Jacquemin D. 2014 How DNA is damaged by external electric fields: selective mutation vs. random degradation. *Phys. Chem. Chem. Phys.* **16**, 8243–8246. (doi:10.1039/C3CP54518K)
 49. Lu Y, Lan Z, Thiel W. 2011 Hydrogen bonding regulates the monomeric nonradiative decay of adenine in DNA strands. *Angewandte Chemie - Int. Ed.* **50**, 6864–6867. (doi:10.1002/anie.201008146)
 50. Cerón-Carrasco JP, Zuñiga J, Requena A, Perpète EA, Michaux C, Jacquemin D. 2011 Combined effect of stacking and solvation on the spontaneous mutation in DNA. *Phys. Chem. Chem. Phys.* **13**, 14 584–14 589. (doi:10.1039/c1cp20946a)
 51. Robbach S, Ochsenfeld C. 2017 Influence of coupling and embedding schemes on QM size convergence in QM/MM approaches for the example of a proton transfer in DNA. *J. Chem. Theory Comput.* **13**, 1102–1107. (doi:10.1021/acs.jctc.6b00727)
 52. Das S, Nam K, Major DT. 2018 Rapid convergence of energy and free energy profiles with quantum mechanical size in quantum mechanical-molecular mechanical simulations of proton transfer in DNA. *J. Chem. Theory Comput.* **14**, 1695–1705. (doi:10.1021/acs.jctc.7b00964)
 53. Kulik HJ, Zhang J, Klinman JP, Martinez TJ. 2016 How large should the QM region be in QM/MM calculations? The case of catechol O-methyltransferase. *J. Phys. Chem.* **120**, 11 381–11 394. (doi:10.1021/acs.jpcc.6b07814)
 54. Podolyan Y, Gorb L, Leszczynski J. 2003 *Ab initio* study of the prototropic tautomerism of cytosine and guanine and their contribution to spontaneous point mutations. *Int. J. Mol. Sci.* **4**, 410–421. (doi:10.3390/i4070410)
 55. Matsui T, Sato T, Shigeta Y, Hirao K. 2009 Sequence-dependent proton-transfer reaction in stacked GC pair II: the origin of stabilities of proton-transfer products. *Chem. Phys. Lett.* **4**, 238–242. (doi:10.1016/j.cplett.2009.07.054)
 56. Laidler KJ, King MC. 1986 Development of transition-state theory. *J. Phys. Chem.* **4**, 2657–2664. (doi:10.1021/j100238a002)

57. Wigner EP. 1932 Über das Überschreiten von Potentialschwellen bei chemischen Reaktionen. *Zeitschrift für Physikalische Chemie* **19B**, 96–109. (doi:10.1515/zpch-1932-0120)
58. Gorb L, Podolyan Y, Leszczynski J, Siebrand W, Fernández-Ramos A, Smedarchina Z. 2002 A quantum-dynamics study of the prototropic tautomerism of guanine and its contribution to spontaneous point mutations in *Escherichia coli*. *Biopolymers* **61**, 77–83. (doi:10.1002/1097-0282(2001)61:1<77::AID-BIP10062>3.0.CO;2-W)
59. Drew HR *et al.* 1981 Structure of a B-DNA dodecamer: conformation and dynamics. *Proc. Natl Acad. Sci. USA* **78**, 2179–2183. (doi:10.1073/pnas.78.4.2179)
60. Elofsson A, Nilsson L. 1993 How consistent are molecular dynamics simulations? Comparing structure and dynamics in reduced and oxidized *Escherichia coli* thioredoxin. *J. Mol. Biol.* **233**, 766–780. (doi:10.1006/jmbi.1993.1551)
61. Caves LSD, Evanseck JD, Karplus M. 1998 Locally accessible conformations of proteins: multiple molecular dynamics simulations of crambin. *Protein Sci.* **7**, 649–666. (doi:10.1002/pro.5560070314)
62. Coveney PV, Wan S. 2016 On the calculation of equilibrium thermodynamic properties from molecular dynamics. *Phys. Chem. Chem. Phys.* **18**, 30236–30240. (doi:10.1039/C6CP02349E)
63. Groen D *et al.* 2019 Introducing VECMAtk—verification, validation and uncertainty quantification for multiscale and HPC simulations. In *Computational Science – ICCS 2019* (eds JMF Rodrigues, PJS Cardoso, J Monteiro, R Lam, VV Krzhizhanovskaya, MH Lees, JJ Dongarra, PMA Sloot), pp. 479–492. Lecture Notes in Computer Science, vol. 11539. Cham, Switzerland: Springer.
64. Galindo-Murillo R, Robertson JC, Zgarbova M, Sponer J, Otyepka M, Jurečka P, Cheatham III TE. 2016 Assessing the current state of Amber force field modifications for DNA. *J. Chem. Theory Comput.* **12**, 4114–4127. (doi:10.1021/acs.jctc.6b00186)
65. Dans PD *et al.* 2016 Long-timescale dynamics of the Drew–Dickerson dodecamer. *Nucleic Acids Res.* **44**, 4052–4066. (doi:10.1093/nar/gkw264)
66. Jorgensen WL, Chandrasekhar J, Madura JD, Impey RW, Klein ML. 1983 Comparison of simple potential functions for simulating liquid water. *J. Chem. Phys.* **79**, 926–935. (doi:10.1063/1.445869)
67. Mangiatordi GF, Brémond E, Adamo C. 2012 DFT and proton transfer reactions: a benchmark study on structure and kinetics. *J. Chem. Theory Comput.* **8**, 3082–3088. (doi:10.1021/ct300338y)
68. Johnson ER, Becke AD. 2006 Van der Waals interactions from the exchange hole dipole moment: application to bio-organic benchmark systems. *Chem. Phys. Lett.* **432**, 600–603. (doi:10.1016/j.cplett.2006.10.094)
69. Otero-De-La-Roza A, Johnson ER. 2013 Non-covalent interactions and thermochemistry using XDM-corrected hybrid and range-separated hybrid density functionals. *J. Chem. Phys.* **138**, 204109. (doi:10.1063/1.4807330)
70. Grimme S. 2011 Density functional theory with London dispersion corrections. *Wiley Interdiscip. Rev. Comput. Mol. Sci.* **1**, 211–228. (doi:10.1002/wcms.30)
71. Jureka P, Šponer J, Černý J, Hobza P. 2006 Benchmark database of accurate (MP2 and CCSD(T) complete basis set limit) interaction energies of small model complexes, DNA base pairs, and amino acid pairs. *Phys. Chem. Chem. Phys.* **8**, 1985–1993. (doi:10.1039/B600027D)
72. Kruse H, Banáš P, Šponer J. 2019 Investigations of stacked DNA base-pair steps: highly accurate stacking interaction energies, energy decomposition, and many-body stacking effects. *J. Chem. Theory Comput.* **15**, 95–115. (doi:10.1021/acs.jctc.8b00643)
73. Xiao S, Wang L, Liu Y, Lin X, Liang H. 2012 Theoretical investigation of the proton transfer mechanism in guanine-cytosine and adenine-thymine base pairs. *J. Chem. Phys.* **137**, 195101. (doi:10.1063/1.4766319)
74. Tolosa S, Sansón JA, Hidalgo A. 2017 Theoretical thermodynamic study of the adenine–thymine tautomeric equilibrium: electronic structure calculations and steered molecular dynamic simulations. *Int. J. Quantum Chem.* **117**, 1–9. (doi:10.1002/qua.25429)
75. Senn HM, Thiel W. 2007 QM/MM methods for biological systems. *Atomistic Approaches Mod. Biol.* **268**, 173–290. (doi:10.1007/128_2006_084)
76. Kästner J, Carr JM, Keal TW, Thiel W, Wander A, Sherwood P. 2009 DL-FIND: an open-source geometry optimizer for atomistic simulations. *J. Phys. Chem. A* **113**, 11856–11865. (doi:10.1021/jp9028968)
77. Boulanger E, Thiel W. 2014 Toward QM/MM simulation of enzymatic reactions with the Drude oscillator polarizable force field. *J. Chem. Theory Comput.* **10**, 1795–1809. (doi:10.1021/ct401095k)
78. Ganguly A, Boulanger E, Thiel W. 2017 Importance of MM polarization in QM/MM studies of enzymatic reactions: assessment of the QM/MM Drude oscillator model. *J. Chem. Theory Comput.* **13**, 2954–2961. (doi:10.1021/acs.jctc.7b00016)
79. Lu Y, Lan Z, Thiel W. 2012 Monomeric adenine decay dynamics influenced by the DNA environment. *J. Comput. Chem.* **33**, 1225–1235. (doi:10.1002/jcc.22952)
80. Henkelman G, Uberuaga BP, Jónsson H. 2000 Climbing image nudged elastic band method for finding saddle points and minimum energy paths. *J. Chem. Phys.* **113**, 9901–9904. (doi:10.1063/1.1329672)
81. Henkelman G, Jónsson H. 1999 A dimer method for finding saddle points on high dimensional potential surfaces using only first derivatives. *J. Chem. Phys.* **111**, 7010–7022. (doi:10.1063/1.480097)
82. Metz S, Kästner J, Sokol AA, Keal TW, Sherwood P. 2014 ChemShell—a modular software package for QM/MM simulations. *Wiley Interdiscip. Rev. Comput. Mol. Sci.* **4**, 101–110. (doi:10.1002/wcms.1163)
83. Tolosa S, Sansón JA, Hidalgo A. 2018 Mechanisms for guanine–cytosine tautomeric equilibrium in solution via steered molecular dynamic simulations. *J. Mol. Liq.* **251**, 308–316. (doi:10.1016/j.molliq.2017.12.091)
84. Mardirossian N, Head-Gordon M. 2017 Thirty years of density functional theory in computational chemistry: an overview and extensive assessment of 200 density functionals. *Mol. Phys.* **115**, 2315–2372. (doi:10.1080/00268976.2017.1333644)
85. Cérón-Carrasco JP, Jacquemin D. 2013 Electric field induced DNA damage: an open door for selective mutations. *Chem. Commun.* **49**, 7578. (doi:10.1039/c3cc42593b)
86. Alberts B, Johnson A, Alexander L, Raff M, Keith R, Walter P. 2002 *Molecular biology of the cell*, 4th edn. New York, NY: Garland Science.
87. Lee H, Popodi E, Tang H, Foster PL. 2012 Rate and molecular spectrum of spontaneous mutations in the bacterium *Escherichia coli* as determined by whole-genome sequencing. *Proc. Natl Acad. Sci. USA* **109**, E2774–E2783. (doi:10.1073/pnas.1210309109)
88. Ossowski S *et al.* 2010 The rate and molecular spectrum in *Arabidopsis thaliana*. *Science* **327**, 92–95. (doi:10.1126/science.1180677)
89. Cheng KC, Cahill DS, Kasai H, Nishimura S, Loeb LA. 1992 8-Hydroxyguanine, an abundant form of oxidative DNA damage, causes G to T and A to C substitutions. *J. Biol. Chem.* **267**, 166–172.
90. Fu LY, Wang GZ, Ma BG, Zhang HY. 2011 Exploring the common molecular basis for the universal DNA mutation bias: revival of Löwdin mutation model. *Biochem. Biophys. Res. Commun.* **409**, 367–371. (doi:10.1016/j.bbrc.2011.05.017)